Electronic Supplementary Material (ESI) for Inorganic Chemistry Frontiers.

Electronic Supplementary Information

Tailoring the Pore Size and Shape of the One-Dimensional Channels in Iron-based MOFs for Enhancing the Methane Storage Capacity

Thach N. Tu,*[a,b] Huong T. D. Nguyen,[c] Nhung T. Tran[d]

[a]Nguyen Tat Thanh University, 300A Nguyen Tat Thanh Street, District 4, Ho Chi Minh City 755414, Vietnam

[b]Vietnam National University-Ho Chi Minh (VNU-HCM), Ho Chi Minh City 721337, Vietnam.

[c]University of Science, Vietnam National University-Ho Chi Minh (VNU-HCM), Ho Chi Minh City 721337, Vietnam

[d]Ho Chi Minh City University of Technology and Education (HCMUTE), 01 Vo Van Ngan Street, Thu Duc District, Ho Chi Minh City 720100, Vietnam

*To whom correspondence should be addressed: tnthach@ntt.edu.vn

Table of Contents

Section S1 Materials and Analytical Techniques

Analytical techniques. A single crystal of Fe-NDC was mounted on a cryoloop then the data set was collected at 297 K using a Bruker D8 Venture diffractometer, in which, X-rays was generated by a monochromatic microfocus Cu K_α radiation source (λ = 1.54178 Å) at 50 kV and 1.0 mA. The diffraction data was collected by a PHOTON-100 CMOS detector. After collecting, the unit cell was then determined by Bruker SMART APEX II software suite. Subsequently, the data set was reduced and data correction was carried out by a multi-scan spherical absorption method. The structure was solved by direct methods and further refinement was carried out using the full-matrix least-squares method in the SHELX-97 program package. After locating the framework backbone atoms, the SQUEEZE routine in PLATON was used to remove residual electron density from solvent molecules inside the pore of Fe-NDC. Due to the small crystal size of Fe-NDC, the maximum resolution could only be obtained at 1.32 Å thus the final structure was isotropically refined using modified electron density map obtained from the SQUEEZE routine. Powder X-ray diffraction (PXRD) patterns were collected using a D8 Advance diffractometer equipped with a LYNXEYE detector. Thermal gravimetric analysis (TGA) was performed using a TA Instruments Q-500 thermal gravimetric analyzer under a gas mixture of O_2 (20%) and N_2 (80%) with temperature ramp of 5 °C min^{-1}. Fourier transform infrared (FT-IR) spectra were measured on a Bruker ALPHA FTIR spectrometer using potassium bromide pellets. Low-pressure N_2 adsorption measurements were carried out on a Quantachrome Autosorb iQ volumetric gas adsorption analyzer. A liquid N_2 bath was used for measurements at 77 K. Helium was used as estimation of dead space. Ultrahigh-purity-grade N_2 and He (99.999% purity) were used throughout adsorption experiments. Elemental analysis of Fe-NDC was performed in the Microanalytical Laboratory of the College of Chemistry at UC Berkeley using a Perkin Elmer 2400 Series II combustion analyzer. High-pressure methane adoption measurements of VNU-21, VNU-22, and Fe-NDC were performed using the micromeritics HPVA 100.

Section S2 Single Crystal X-ray Diffraction Analysis

Table S1. Crystal data and structure refinement for Fe-NDC

Empirical formula	$Fe_3C_{30}H_{12}N_2O_{17.64}S$
Formula weight	882.27
Temperature (K)	150
Wavelength (Å)	1.54178
Crystal system	Tetragonal
Space group	*P4/nmm*
Unit cell dimensions (Å)	*a* = 17.670(3)
	b = 17.670(3)
	c = 8.0543(16)
Volume ($Å^3$)	2514.8(11)
Z	2
Density ($g\ cm^{-1}$)	1.169
Absorption coefficient (mm^{-1})	7.749
F(000)	882
Crystal size (mm)	0.15 × 0.05× 0.03
θ range (°)	$3.537 \le \theta \le 35.862$
Index ranges	$-11 \le h \le 13$; $-12 \le k \le 13$; $-5 \le l \le 6$
Reflections collected	3892
Independent reflections	342
Completeness to θ = 35.862 °	0.980
Data / restraints / parameters	3892/0/ 64
S (GOF)	1.606
R_1, wR_2 [$I > 2\sigma(I)$]	R_1 = 0.1424, wR_2 = 0.3451
R_1, wR_2 (all data)	R_1 = 0.1807, wR_2 = 0.3700
Largest diff. peak and hole ($e \cdot Å^{-3}$)	0.492, -0.608

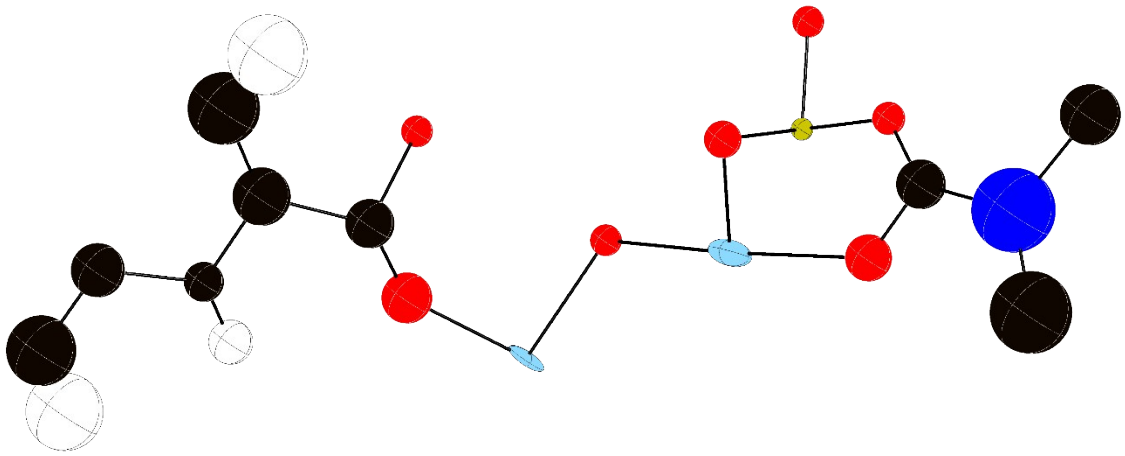

Figure S1 Thermal ellipsoid plot of the asymmetric unit of Fe-NDC with 30% probability. C, black; O, red; Fe, light blue; S, yellow; N, blue; H, white.

Section S3 Structural Description

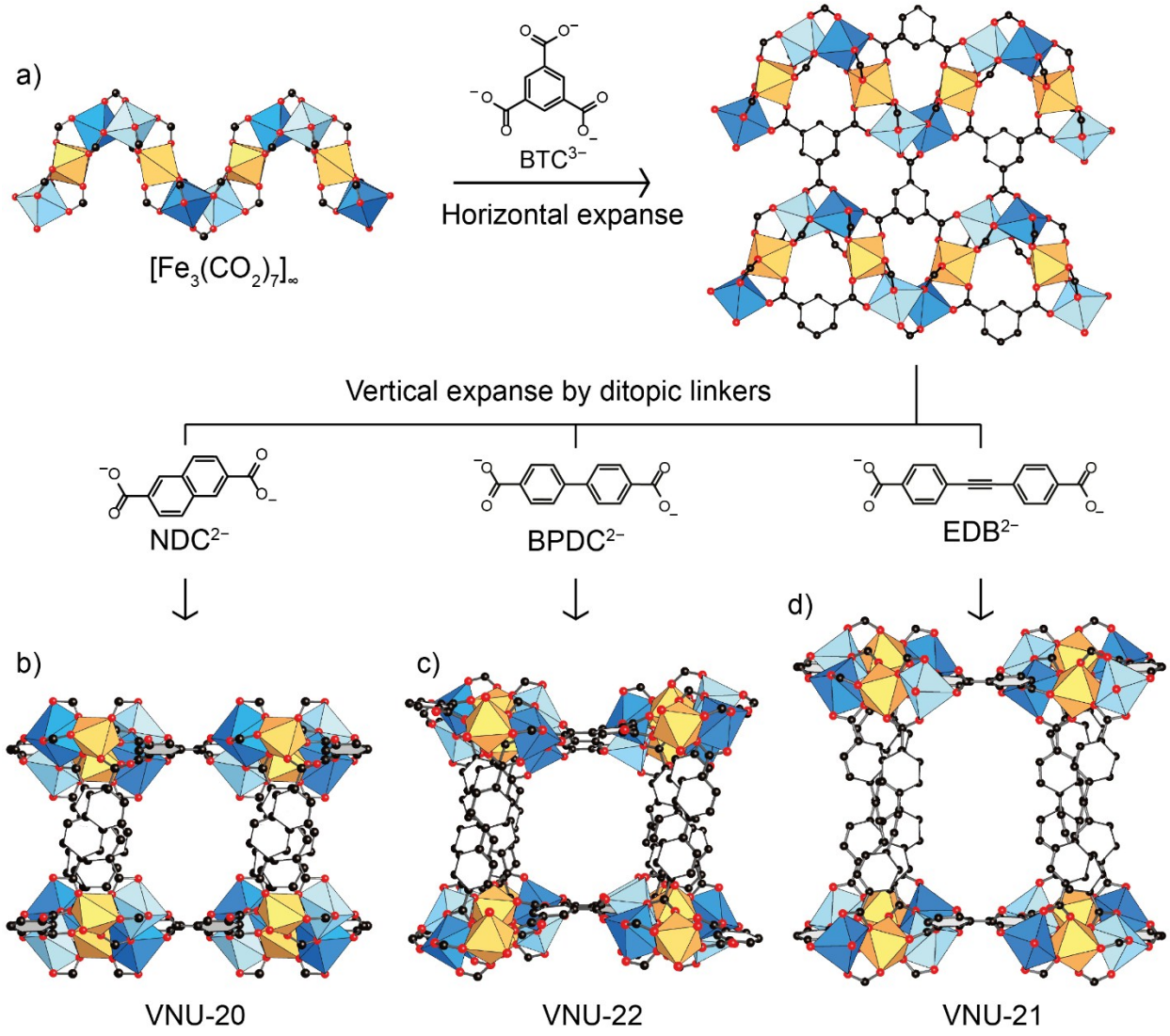

Figure S2 The structures of VNU-20, VNU-21 and VNU-22 are composed of the sinusoidal $[Fe_3(CO_2)_7]_\infty$ rod-shaped SBUs (a) linked by BTC^{3-} and the ditopic linkers (NDC^{2-}, $BPDC^{2-}$ or EDB^{2-}) to form the three-dimensional architecture with adjustable size and shape of the 1D channel (b, c, d). Atom colour: Fe, blue and orange octahedra; C, black; O, red. All other H atoms are omitted for clarity.

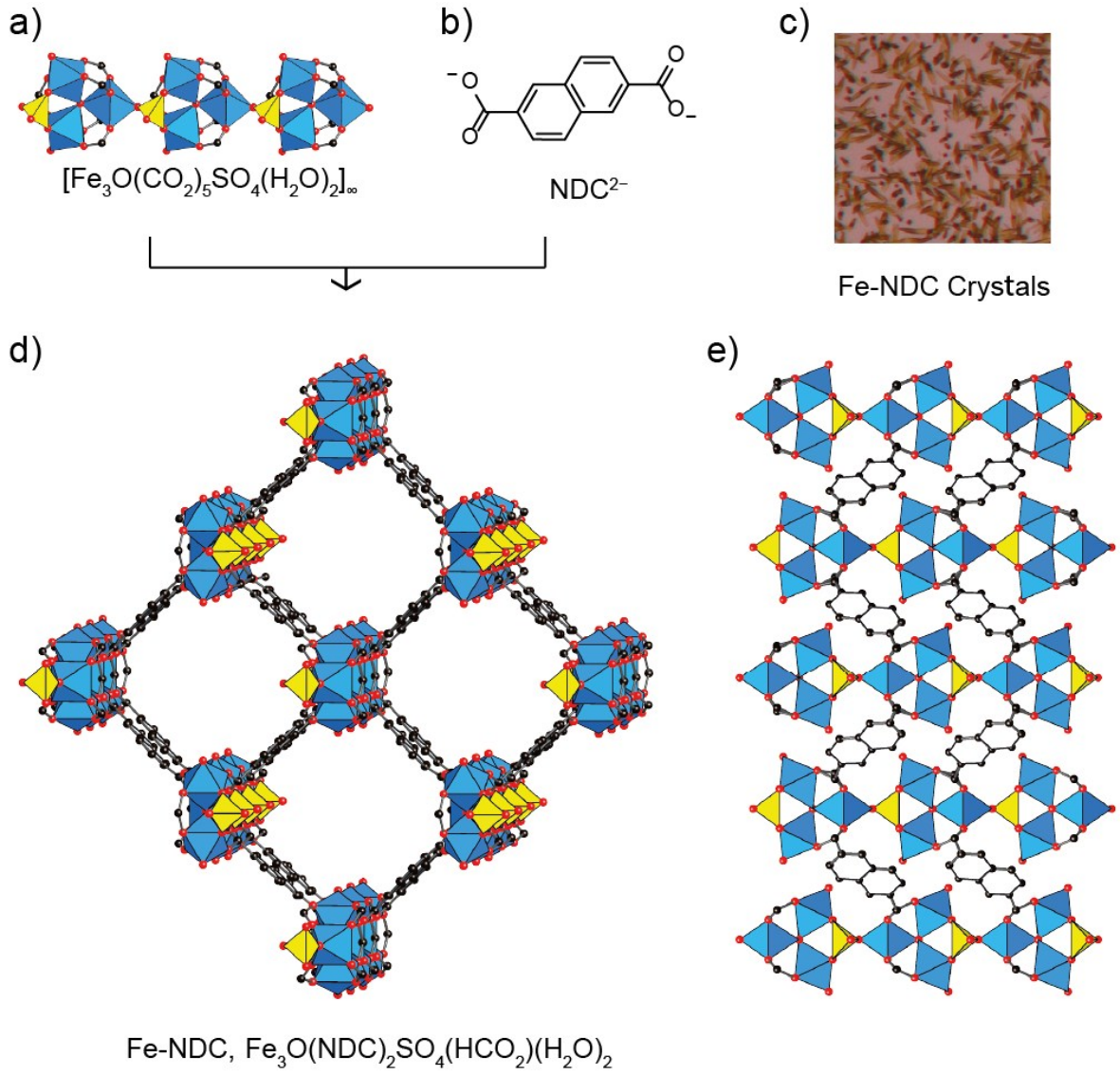

Figure S3 The crystals of Fe-NDC (c) is synthesized from $[Fe_3O(CO_2)_5(SO_4)(H_2O)_2]_\infty$ rod-shaped SBUs (a) and NDC^{2-} linkers (b) to form the three-dimensional architecture (d, e). The structure is shown along Oz (d) and Ox axes (e). Fe, Blue; C, black; O, red; S, yellow. All other H atoms are omitted for clarity.

Section S4 Powder X-ray Diffraction Patterns

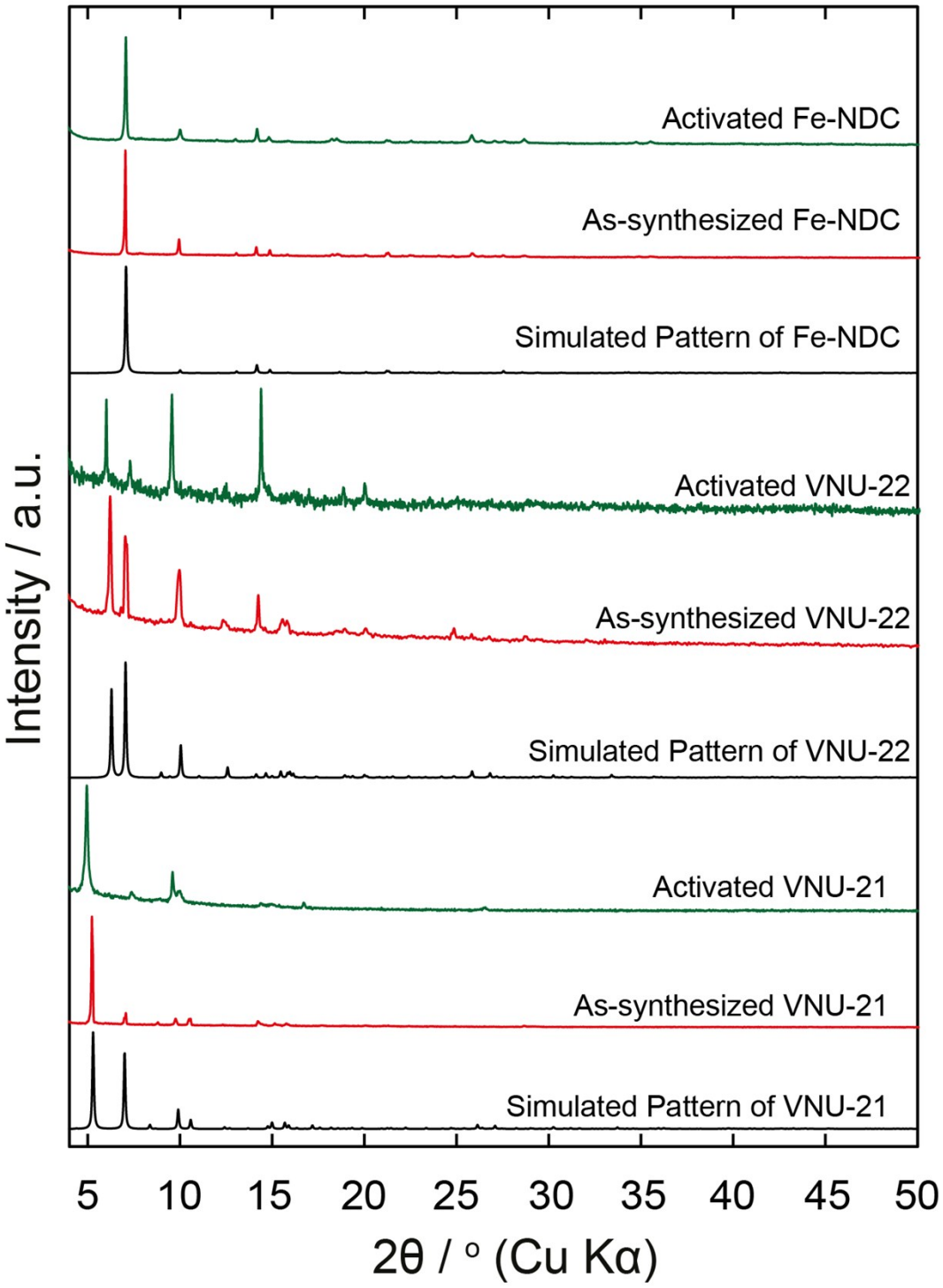

Figure S4 The simulated PXRD patterns of VNU-21, VNU-22, and Fe-NDC from single crystal data (black) compared with the experimental patterns from the as-synthesized samples (red) and samples after activation (green).

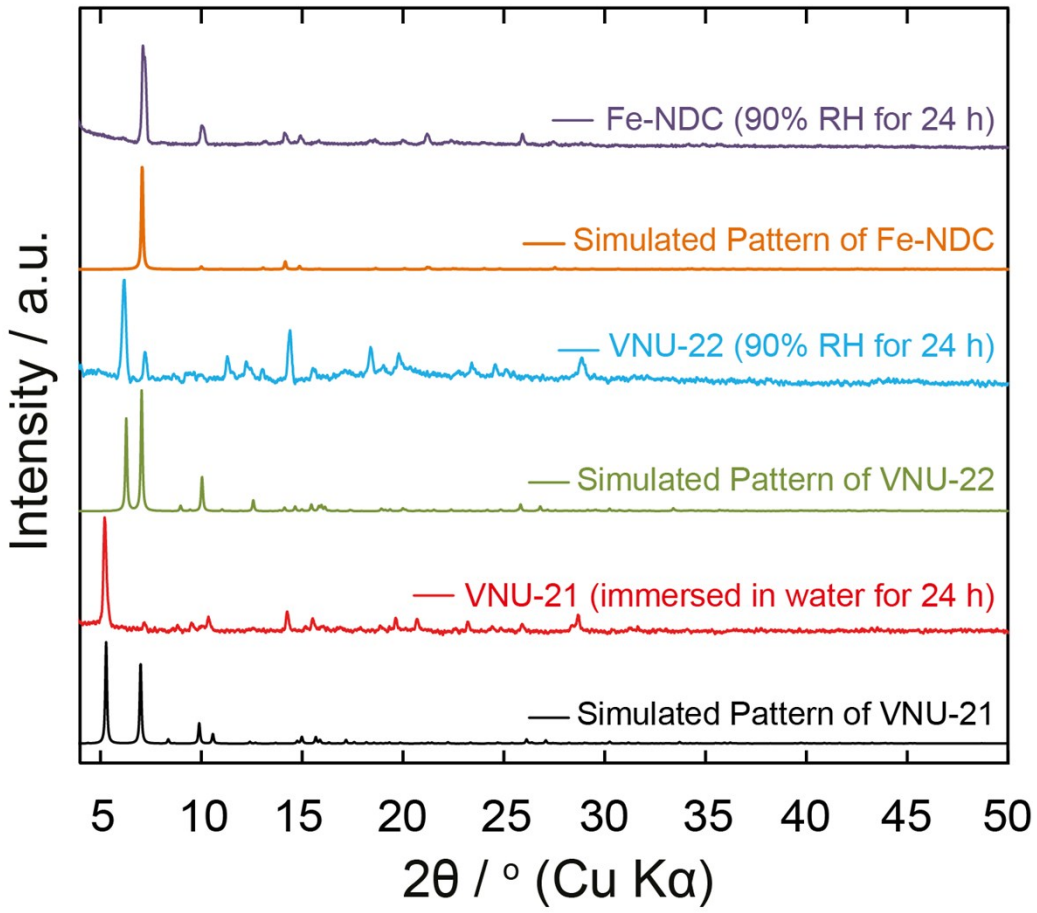

Figure S5 The simulated PXRD patterns of VNU-21, VNU-22, and Fe-NDC from single crystal data in comparison with the experimental patterns of the water-immersed sample of VNU-21 and the other samples (VNU-22 and Fe-NDC), which were treated in the moisture environment (relative humidity = 90%).

Section S5 Fourier Transform Infrared Analysis (FT-IR)

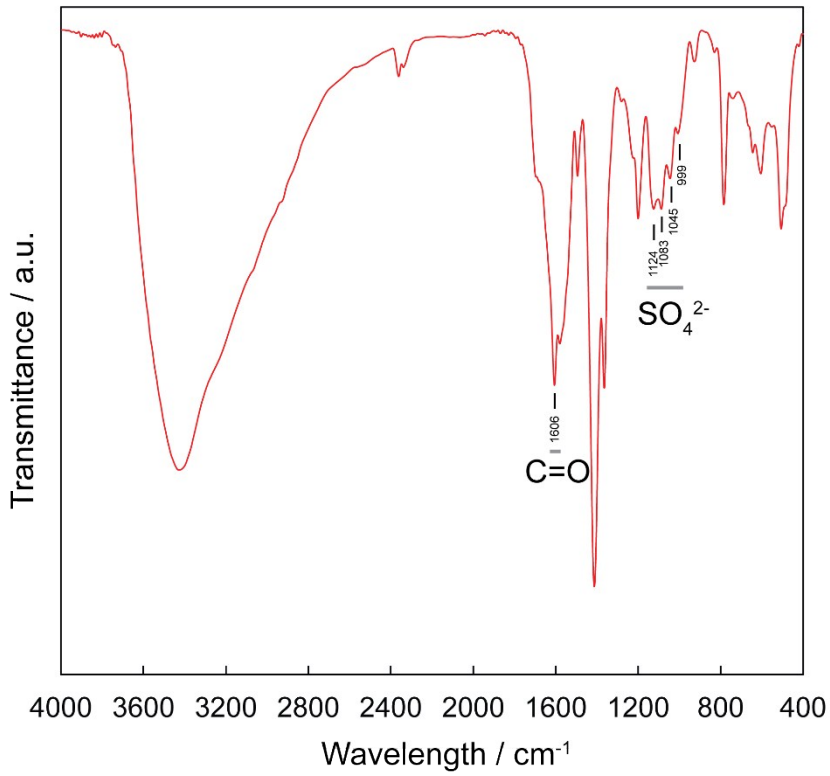

Figure S6 FT-IR spectrum of activated Fe-NDC.

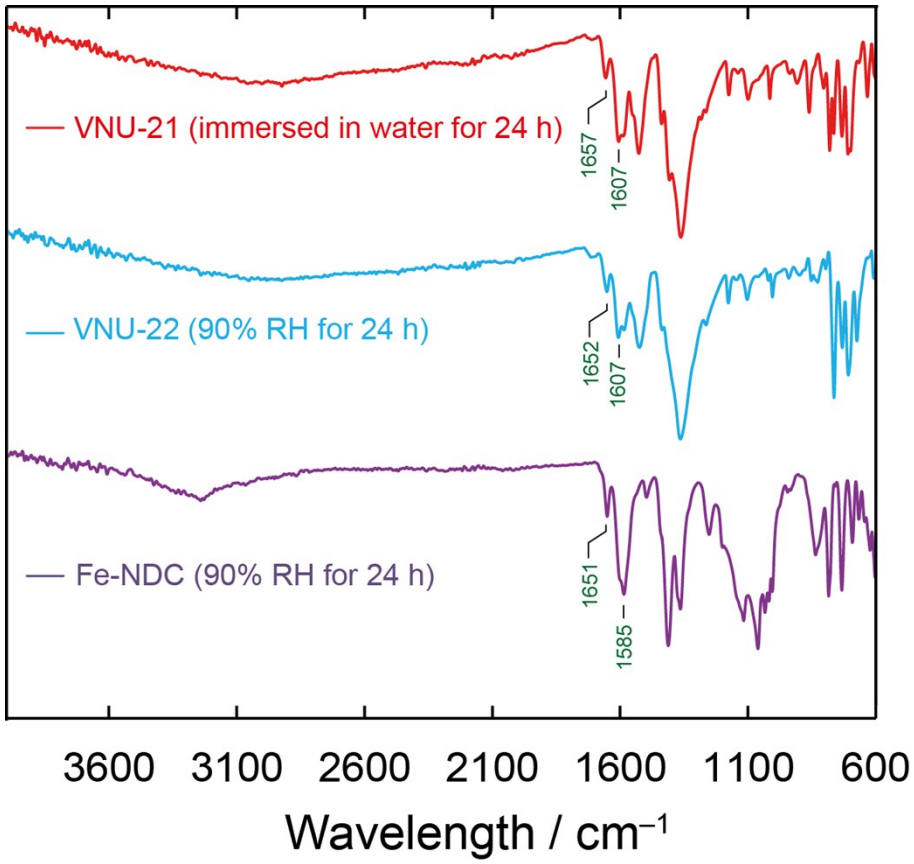

Figure S7 FT-IR spectra of the water-immersed sample of VNU-21 and the other samples (VNU-22 and Fe-NDC), which were treated in the moisture environment (relative humidity = 90%). The absence of free carboxylic acid peaks (≈ 1700 cm^{-1}) in the FT-IR spectra implied the full maintenance of the atomic connectivity of VNU-21, VNU-22 and Fe-NDC without exfoliation after investigation.

Section S6 Thermal Gravimetric Analysis (TGA)

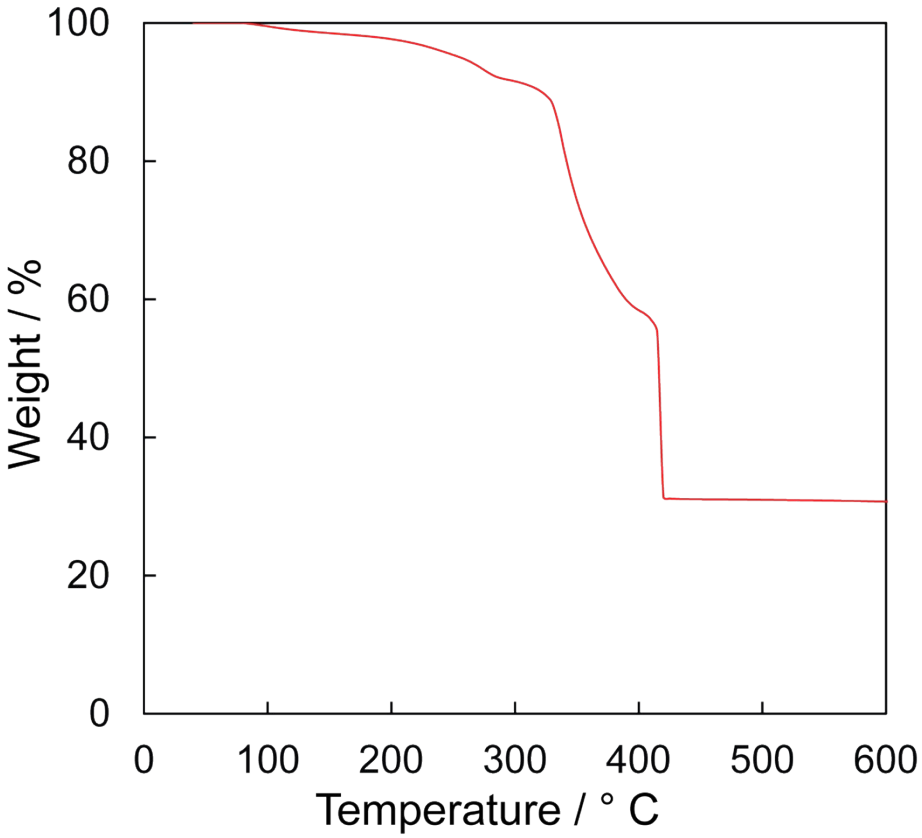

Figure S8 TGA trace showed that Fe-NDC is stable up to 300 °C and the weight percentage of the residual oxide (assigned to Fe_2O_3) is consistent with the theoretical value calculated from the modelled structure (31.0 and 33.9 wt%, respectively).

Section S7 77 K N_2 Isotherms and Surface Area

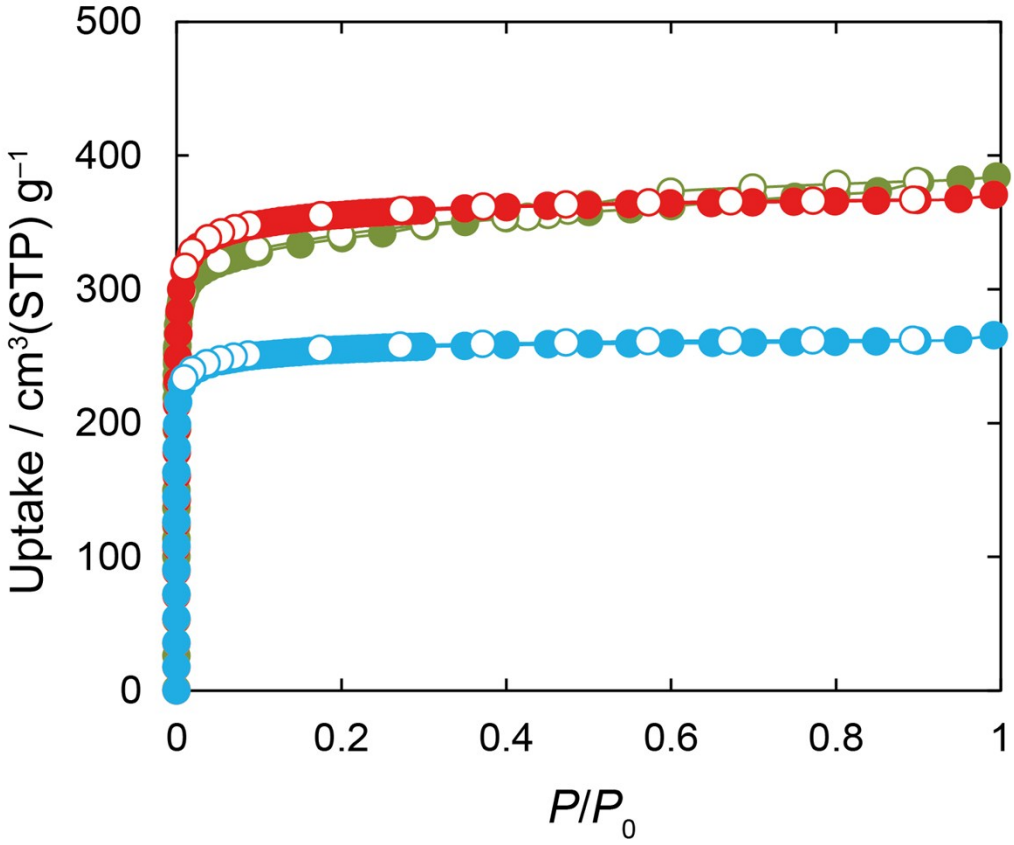

Figure S9 77 K N_2 uptake of VNU-21 (red), VNU-22 (blue) and Fe-NDC (green). The closed and open circles represent the adsorption and desorption branches of the isotherm, respectively. The connecting line functions as a guide for the eye.

Section S8 Low Pressure Gas Adsorption Studies

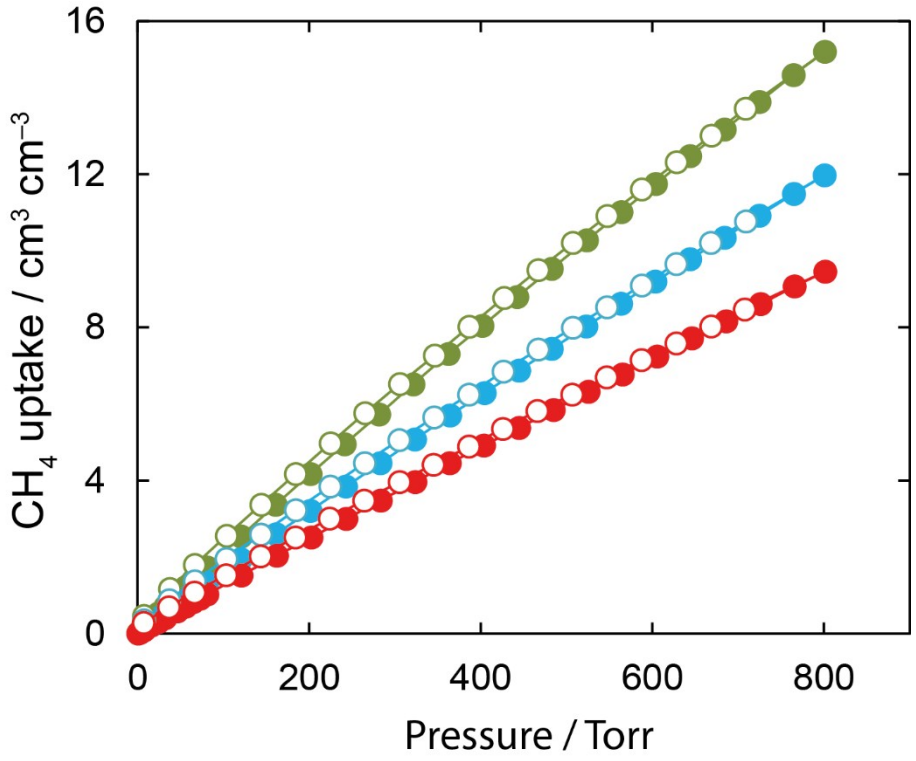

Figure S10 Excess CH_4 uptakes of VNU-21 at 25 °C (red), 15 °C (blue) 5 °C (green).

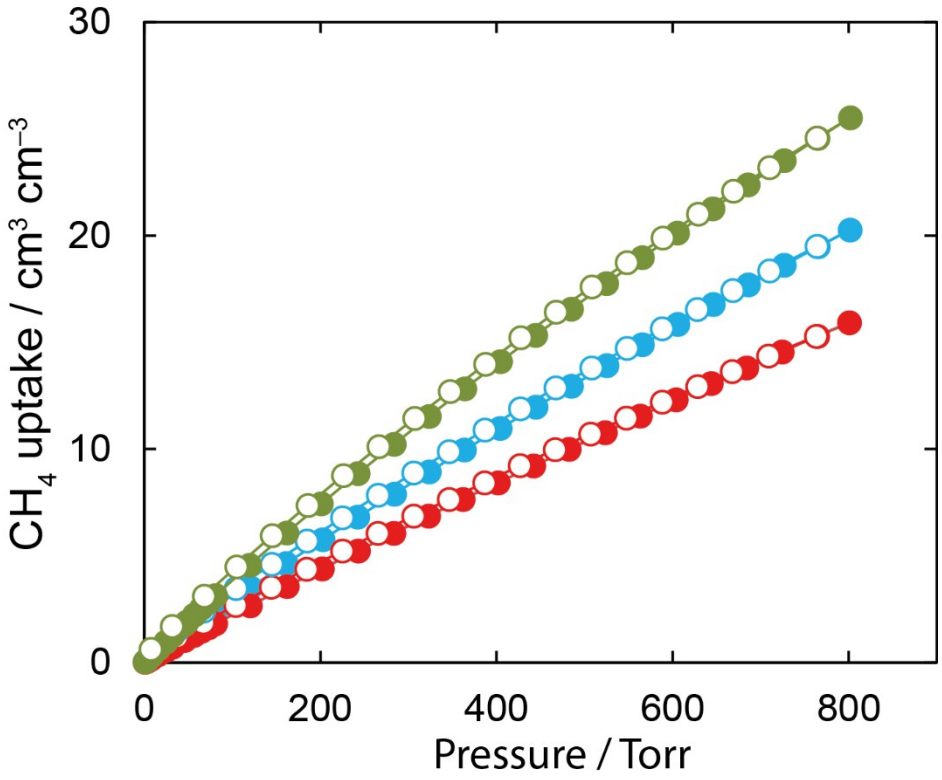

Figure S11 Excess CH_4 uptakes of VNU-22 at 25 °C (red), 15 °C (blue) 5 °C (green).

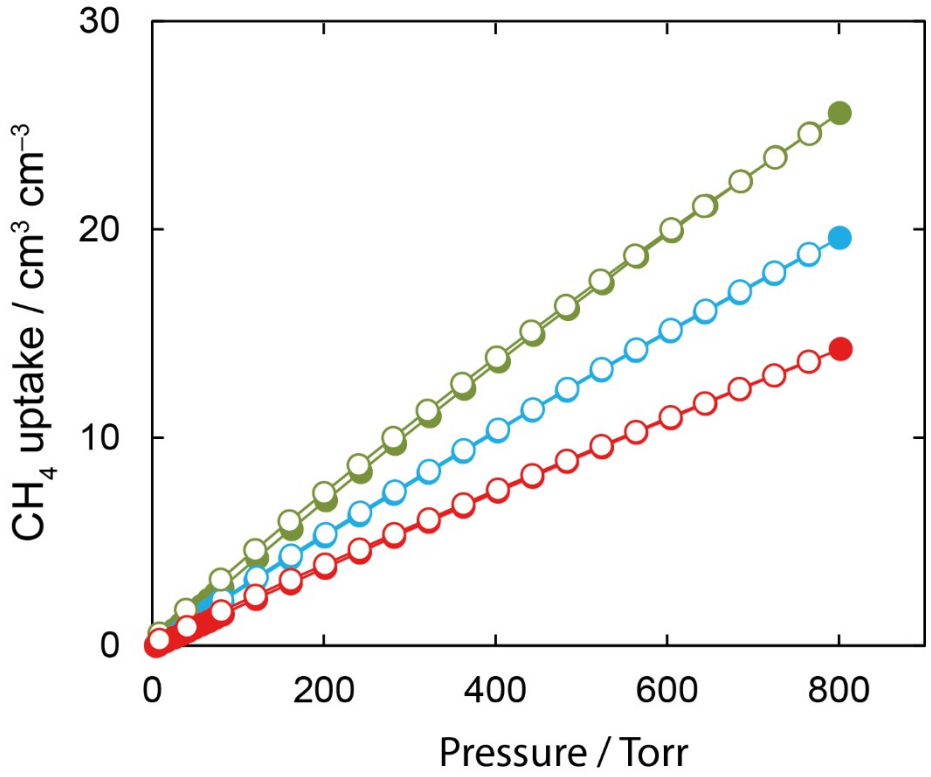

Figure S12 Excess CH_4 uptakes of Fe-NDC at 25 °C (red), 10 °C (blue) 0 °C (green).

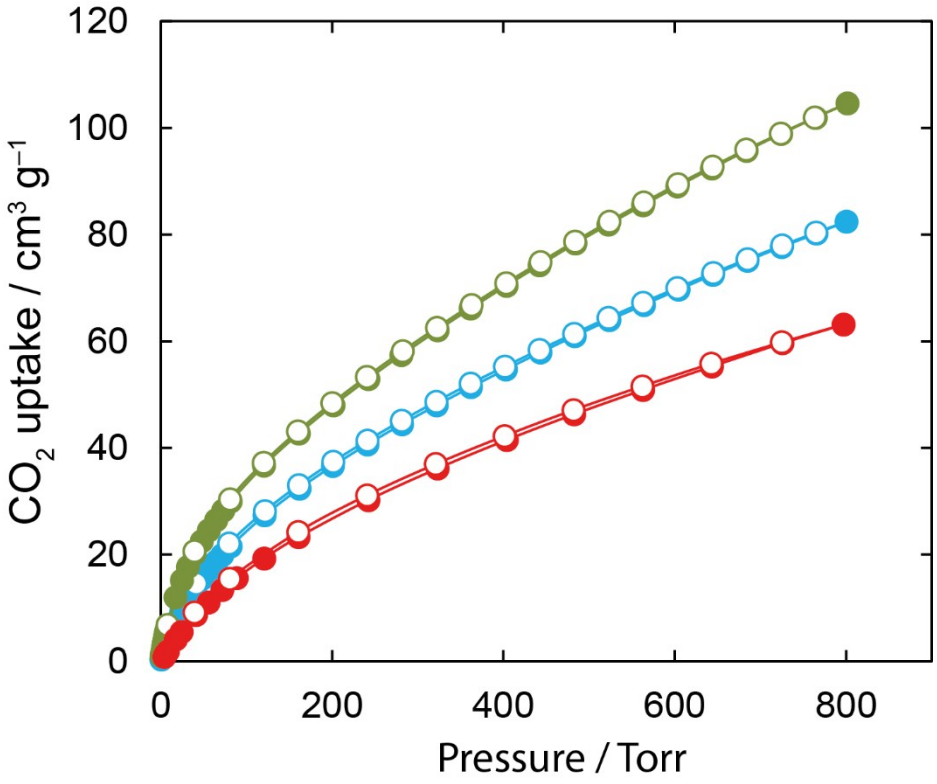

Figure S13 CO_2 uptakes of Fe-NDC at 25 °C (red), 10 °C (blue) 0 °C (green).

Section S9 High Pressure Gas Adsorption Studies

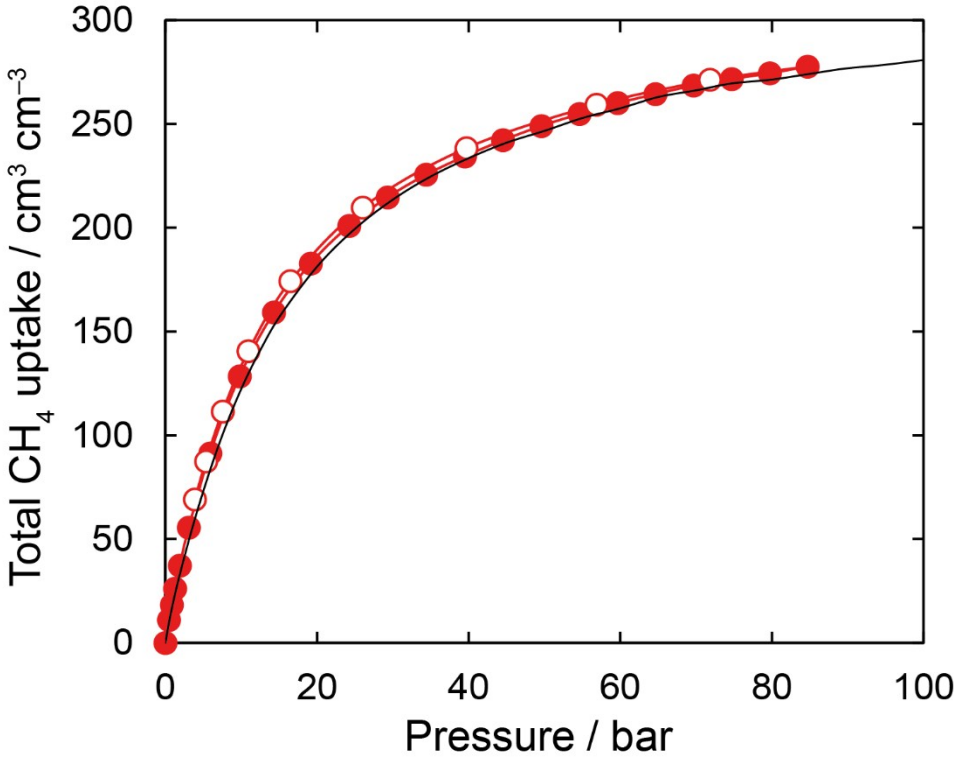

Figure S14 Our measured methane uptake isotherm of HKUST-1 at 25 °C (red) in comparison with that provided by Long *et al* (black line).[1]

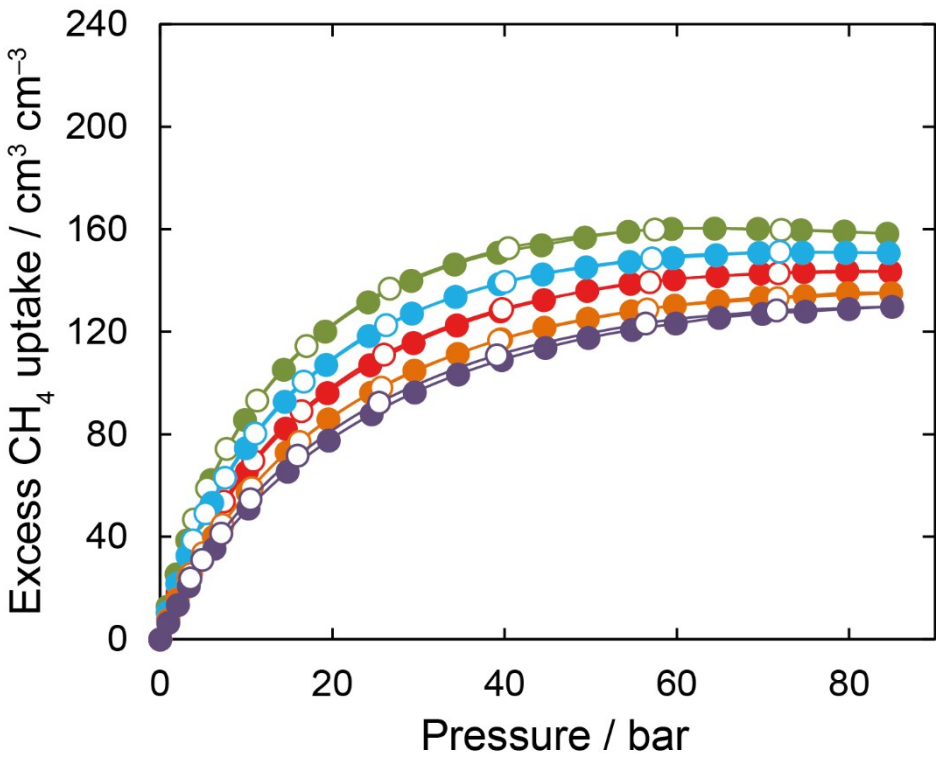

Figure S15 Excess methane uptakes of VNU-21 at 45 °C (purple), 35 °C (orange), 25 °C (red), 15 °C (blue) 5 °C (green).

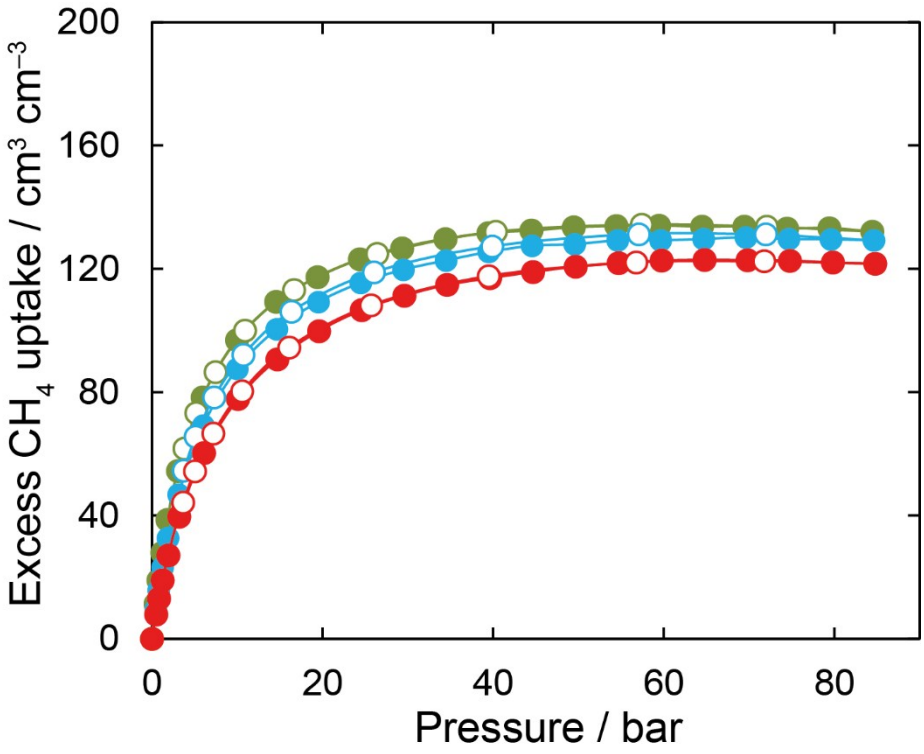

Figure S16 Excess methane uptakes of VNU-22 at 25 °C (red), 15 °C (blue) 5 °C (green).

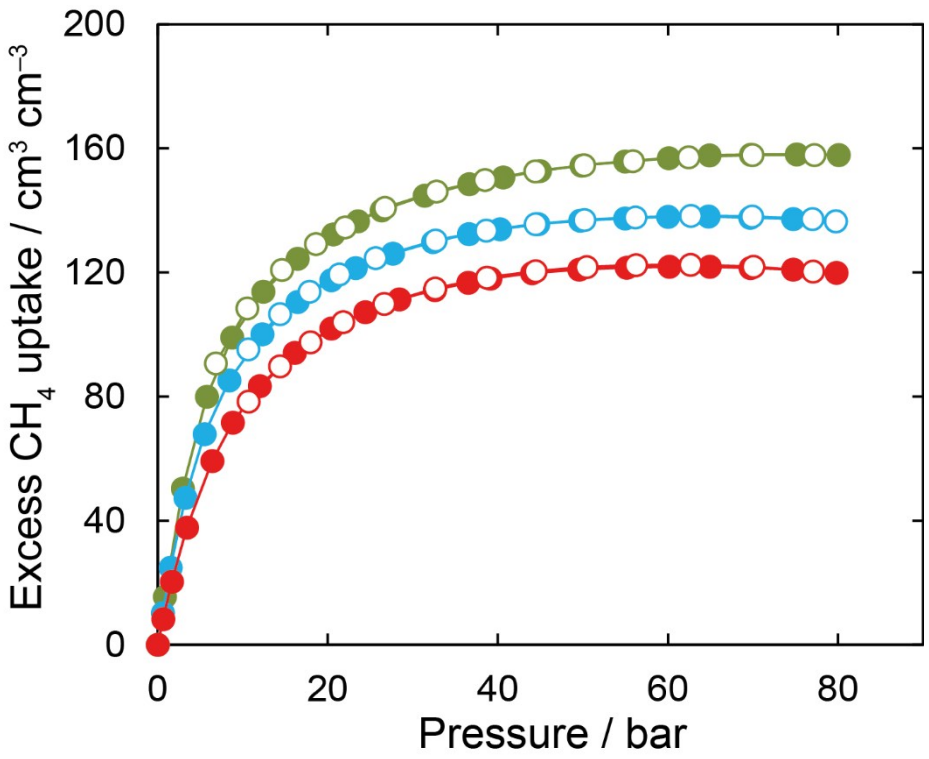

Figure S17 Excess methane uptakes of Fe-NDC at 25 °C (red), 10 °C (blue) 0 °C (green).

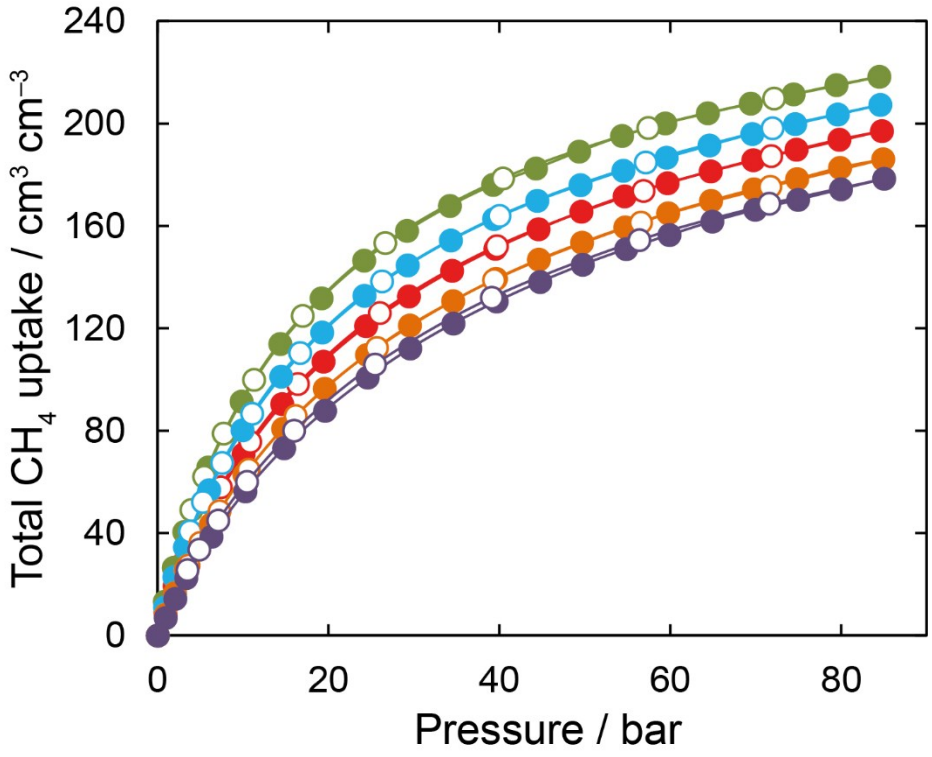

Figure S18 Total methane uptakes of VNU-21 at 45 °C (purple), 35 °C (orange), 25 °C (red), 15 °C (blue) 5 °C (green).

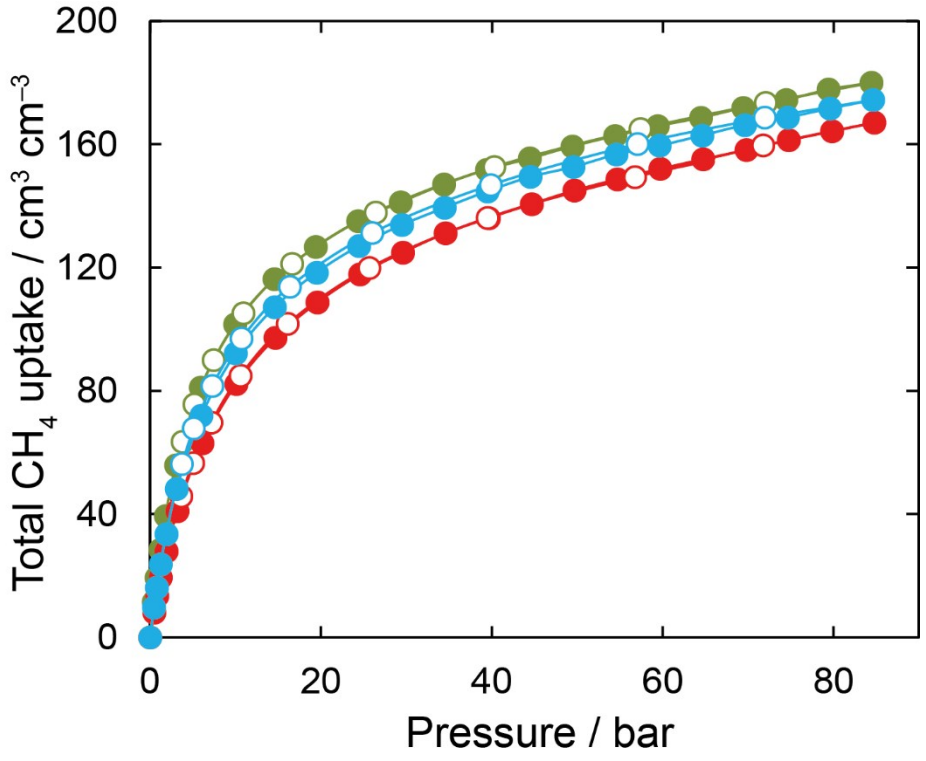

Figure S19 Total methane uptakes of VNU-22 at 25 °C (red), 15 °C (blue) 5 °C (green).

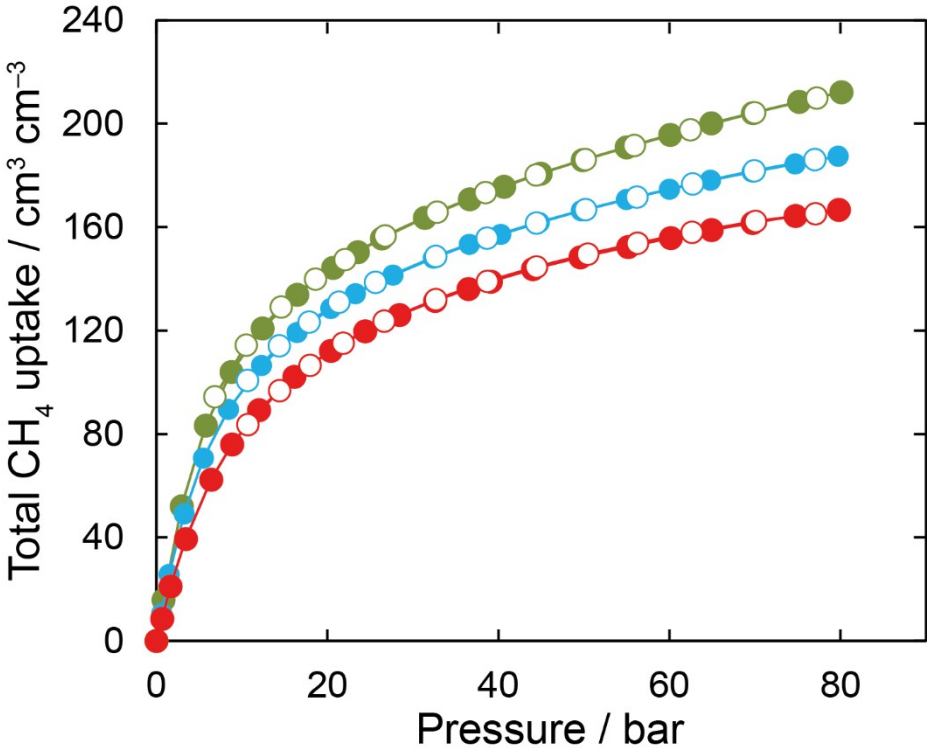

Figure S20 Total methane uptakes of Fe-NDC at 25 °C (red), 10 °C (blue) 0 °C (green).

Section S10 Isosteric Enthalpy of Adsorption

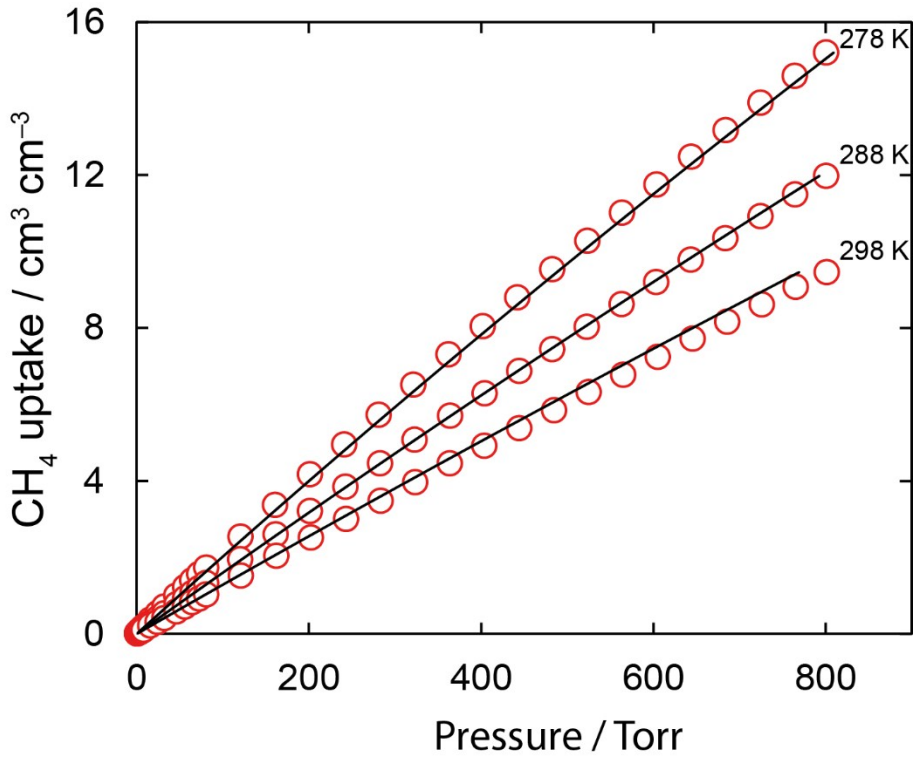

Figure S21 CH_4 adsorption isotherms of VNU-21 (red cycle) in comparison with the Clausius−Clapeyron equation fitting-isotherms (black line).

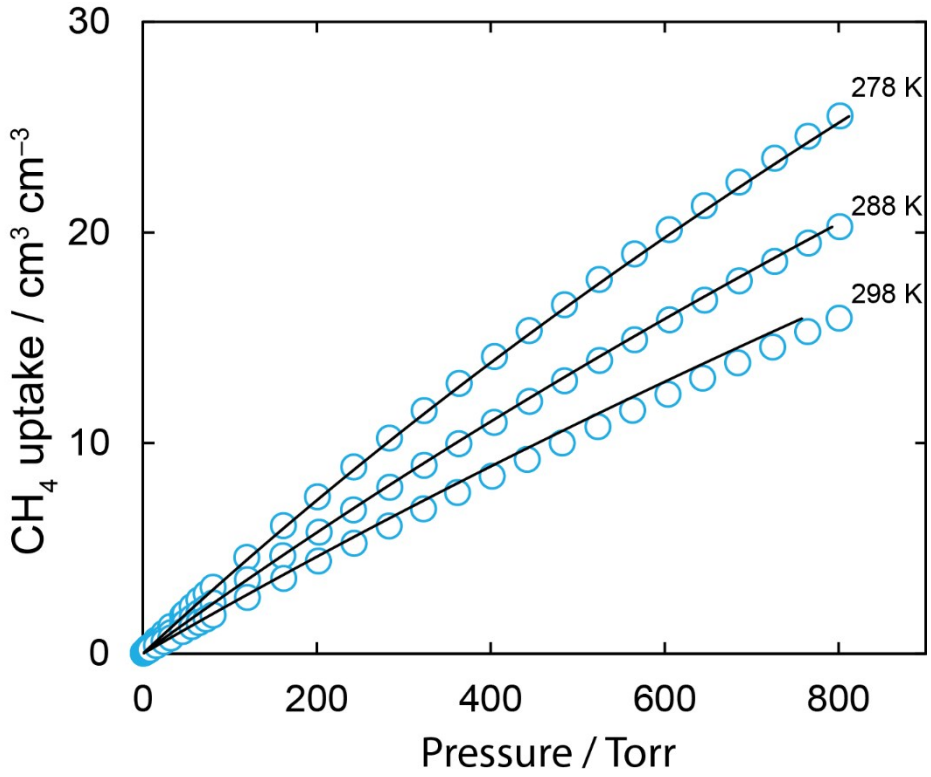

Figure S22 CH_4 adsorption isotherms of VNU-22 (blue cycle) in comparison with the Clausius−Clapeyron equation fitting-isotherms (black line).

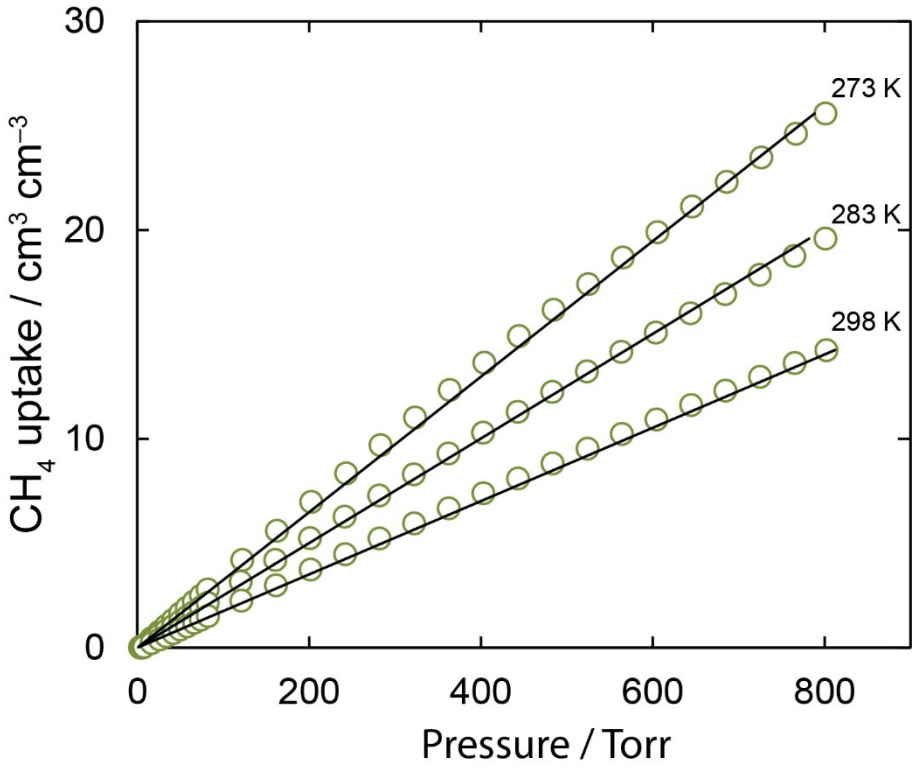

Figure S23 CH_4 adsorption isotherms of Fe-NDC (green cycle) in comparison with the Clausius−Clapeyron equation fitting-isotherms (black line).

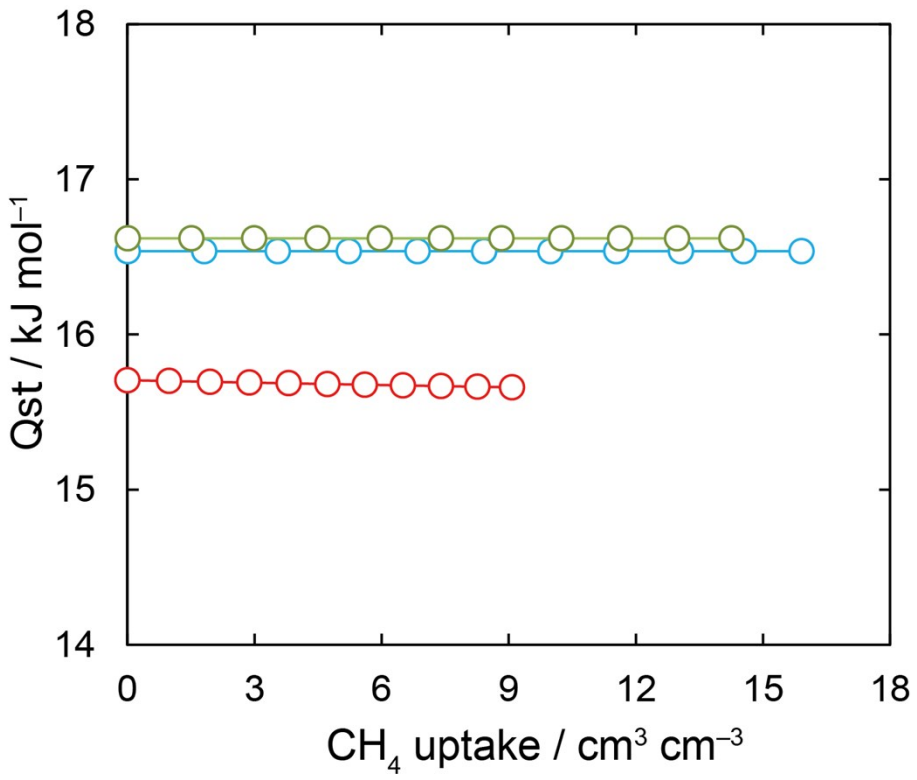

Figure S24 The isosteric heat of methane adsorptions (Qst) for VNU-21 (red), VNU-22 (blue) and Fe-NDC (green) as a function of the methane coverage.

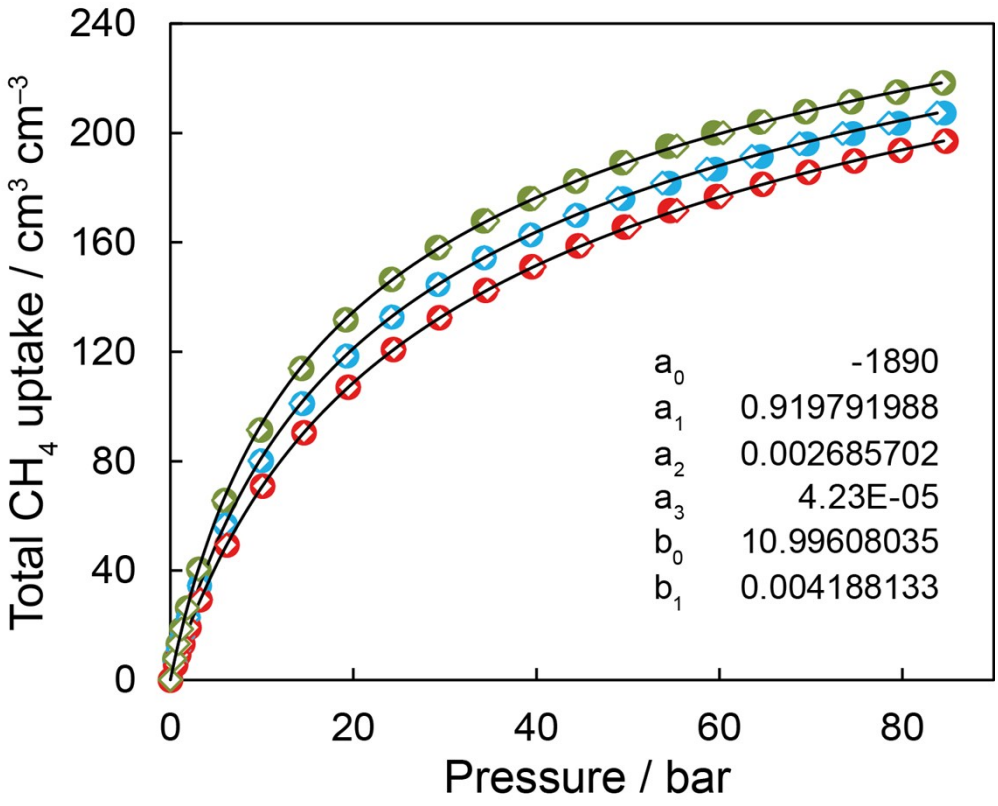

Figure S25 The methane adsorption isotherms of VNU-21 at 25 °C (red circle), 15 °C (blue circle), 5 °C (green circle) in comparison with the Clausius−Clapeyron equation fitting-isotherms at 25 °C (red square), 15 °C (blue square) and 5 °C (green square). Accordingly, the average error between the experimental and fitting-isotherms is 1.3%.

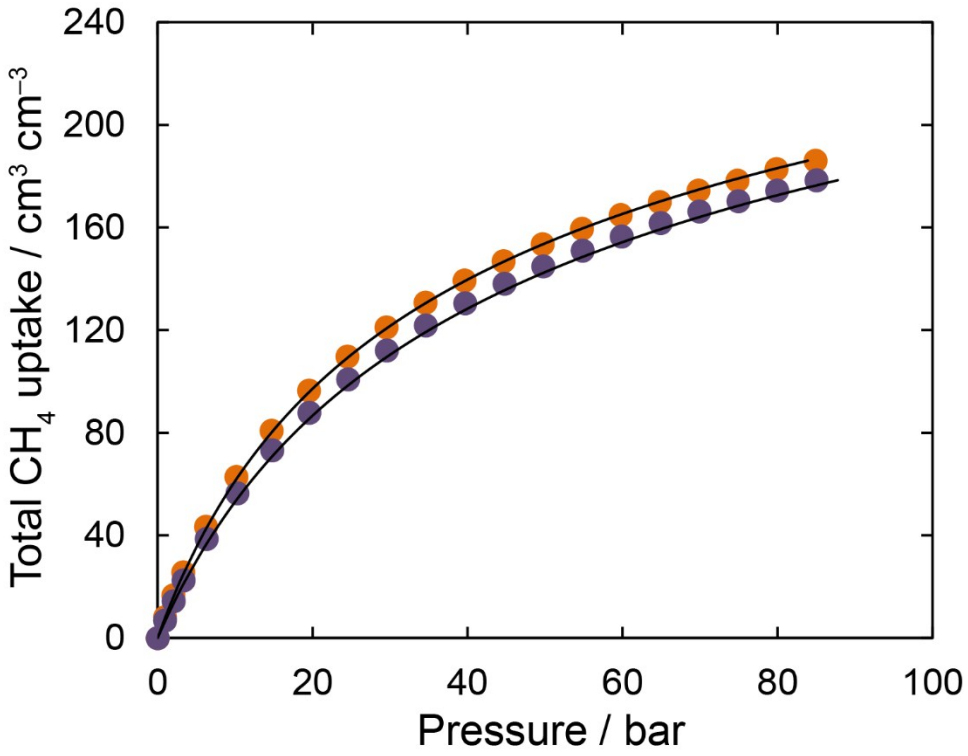

Figure S26 The experimental methane adsorption isotherms of VNU-21 at 35 °C (orange circle), 45 °C (purple circle) in comparison with the calculated isotherms at 35 °C, 45 °C (black lines) derived from the Clausius−Clapeyron equation using parameters obtained from fitting the equation with the isotherms at 5 ≤ T ≤ 25 °C. Accordingly, the average errors between the experimental and calculated isotherms is 3.3%.

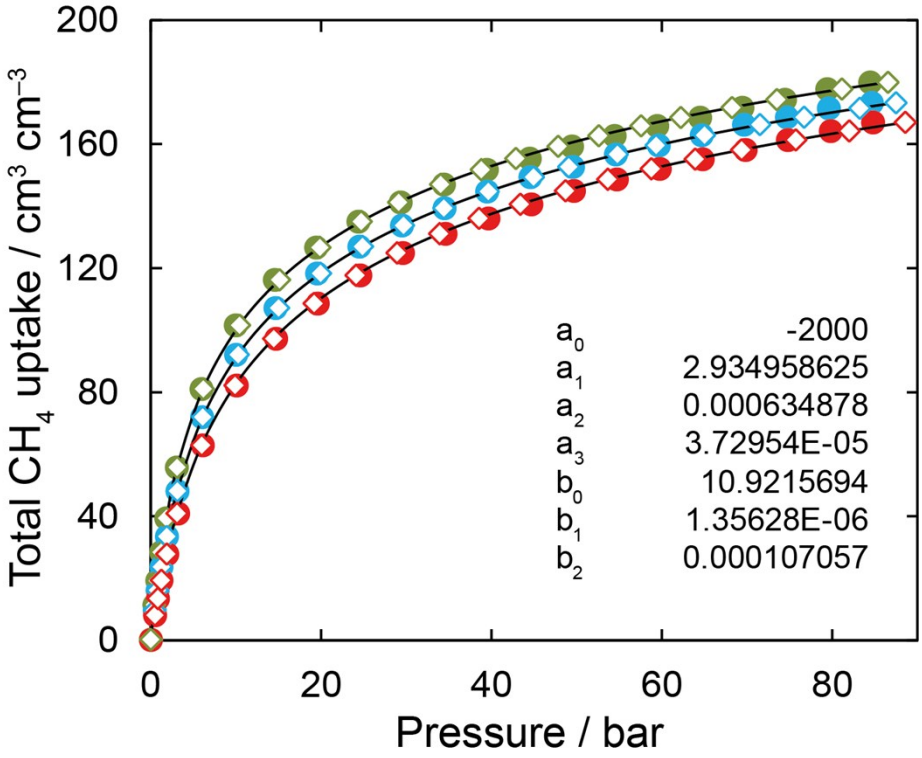

Figure S27 The methane adsorption isotherms of VNU-22 at 25 °C (red circle), 15 °C (blue circle), 5 °C (green circle) in comparison with the Clausius−Clapeyron equation fitting-isotherms at 25 °C (red square), 15 °C (blue square) and 5 °C (green square). Accordingly, the average error between the experimental and fitting-isotherms is 2%.

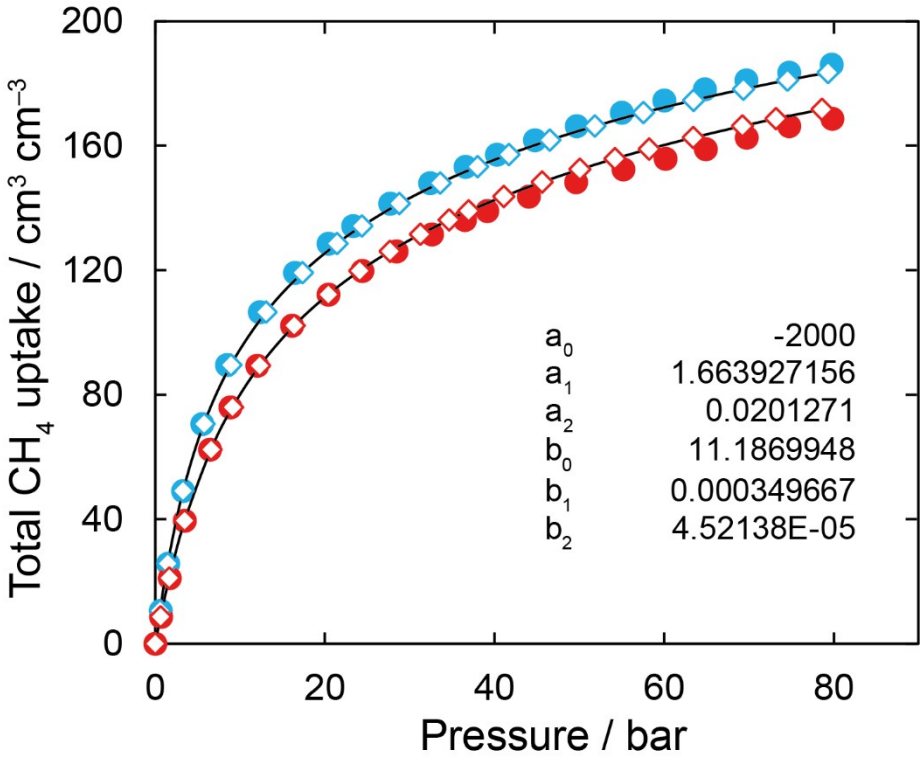

Figure S28 The total adsorption isotherms of Fe-NDC at 25 °C (red circle), 10 °C (blue circle), in comparison with the Clausius−Clapeyron equation fitting-isotherms at 25 °C (red square), 10 °C (blue square). Accordingly, the average error between the experimental and fitting-isotherms is 5%.

References

1. J. A. Mason, M. Veenstra and J. R. Long, *Chem. Sci.*, 2014, **5**, 32–51.